Optical Thouless pumping transport and nonlinear switching in a topological low-dimensional discrete nematic liquid crystal array

Pawel S. Jung,^{1,2,*} Midya Parto,¹ Georgios G. Pyrialakos,¹ Hadiseh Nasari,^{1,3} Katarzyna Rutkowska⁰,² Marek Trippenbach,⁴ Mercedeh Khajavikhan,^{1,3,5} Wieslaw Krolikowski,^{6,7} and Demetrios N. Christodoulides¹

¹CREOL, The College of Optics and Photonics, University of Central Florida, Orlando, Florida 32816, USA

²Faculty of Physics, Warsaw University of Technology, Warsaw, Poland

³Ming Hsieh Department of Electrical and Computer Engineering, University of Southern California, Los Angeles, California 90089, USA

⁴Faculty of Physics, University of Warsaw, Warsaw, Poland

⁵Department of Physics & Astronomy, Dornsife College of Letters, Arts, & Sciences, University of Southern California, Los Angeles, California 90089, USA

⁶Laser Physics Centre, Research School of Physics, Australian National University, Canberra, ACT 0200, Australia

⁷Science Program, Texas A&M University at Qatar, Doha, Qatar



(Received 1 November 2021; accepted 23 December 2021; published 12 January 2022)

We theoretically investigate a Thouless pumping scheme in the one-dimensional topological Su-Schrieffer-Heeger (SSH) model for single and multiple band-gap systems when implemented in a discrete nematic liquid crystal arrangement. For an electrically controlled SSH waveguide array, we numerically demonstrate edge-to-edge light transport at low power levels. On the other hand, at higher powers, the transport is frustrated by light-induced nonlinear defect states, giving rise to robust all-optical switching.

DOI: 10.1103/PhysRevA.105.013513

Topologically protected transport is among the principal hallmarks of topological insulators (TIs) [1-6], which are materials that exhibit an insulating behavior in their bulk, while allowing electron conduction via midgap topologically protected edge states on the surface. This protection is naturally manifested in photonic two-dimensional TIs in the presence of structural imperfections or disorder where the chiral edge modes are immune to backscattering [7-12], thus ensuring a one-way light transport. On the other hand, in one-dimensional topological settings, like that associated with the Su-Schrieffer-Heeger (SSH) model [13], the edge states are zero dimensional and therefore exhibit no transport properties. However, by using topological pumping schemes (in either space or time) one may be able to artificially increase the dimensionality of a given topological configuration. For example, Thouless pumping protocols [14] can provide a route for edge to edge light transport even in one-dimensional systems [15,16], which happens to be robust against random defects. Within the context of photonics, such Thouless schemes have been recently demonstrated in one-dimensional (1D) waveguide arrays [17–19]. Furthermore, the concept of non-Abelian Thouless pumping in a photonic lattice has also been lately proposed [20].

The functionality of topological systems can be greatly enhanced by utilizing nonlinear interactions. Liquid crystals (LCs), are known for their strong nonlinearities and thus can be of use in topological photonics [21]. In nematic liquid crystals (NLCs), the nonlinearity results from molecular reorientation and can be externally tuned via electric [22] or

magnetic fields [23]. These attributes, combined with topological configurations can open new vistas for novel low-power all-optical steering elements that are robust to perturbations [24,25].

In this work, we theoretically investigate the response of an optical liquid-crystal-based topological SSH model in the presence of adiabatic Thouless pumping. In this respect, we provide a design involving a periodic electrode pattern in the NLC planar cell in order to emulate the SSH array that is known to support topologically protected states. In addition, we introduce a *z*-dependent electrode design in order to implement the Thouless pumping scheme. Finally, by using nonlinearity as another degree of freedom, we break the chiral symmetry of the system, thus allowing light switching between topological and trivial defect states.

We start with a brief discussion of the simple 1D non-trivial SSH polyacetylene model, as schematically shown in Figs. 1(a) and 1(b). This model is known to describe particle hopping on a one-dimensional chain, with staggered hopping amplitudes (t_A and t_B). This finite chain possesses two species A and B, spanning in total M sites. Within the tight-binding formalism, the dynamics in this SSH configuration can be described by the following Hamiltonian [26]:

$$\widehat{H} = M_A \sum_{n=1}^{M} \widehat{c}_n^{A\dagger} \widehat{c}_n^A + M_B \sum_{n=1}^{M} \widehat{c}_n^{B\dagger} \widehat{c}_n^B$$

$$+ \sum_{n=1}^{M} (\widehat{c}_n^{B\dagger} \widehat{c}_n^A + \widehat{c}_n^{A\dagger} \widehat{c}_n^B) t_A + (\widehat{c}_{n-1}^{B\dagger} \widehat{c}_n^A + \widehat{c}_n^{A\dagger} \widehat{c}_{n-1}^B) t_B, \quad (1)$$

where $\widehat{c}_n^A \dagger$, $\widehat{c}_n^B \dagger$ and \widehat{c}_n^A , \widehat{c}_n^B denote creation and annihilation operators at site n in the sublattices A and B, respectively, while

^{*}pawel.jung@ucf.edu

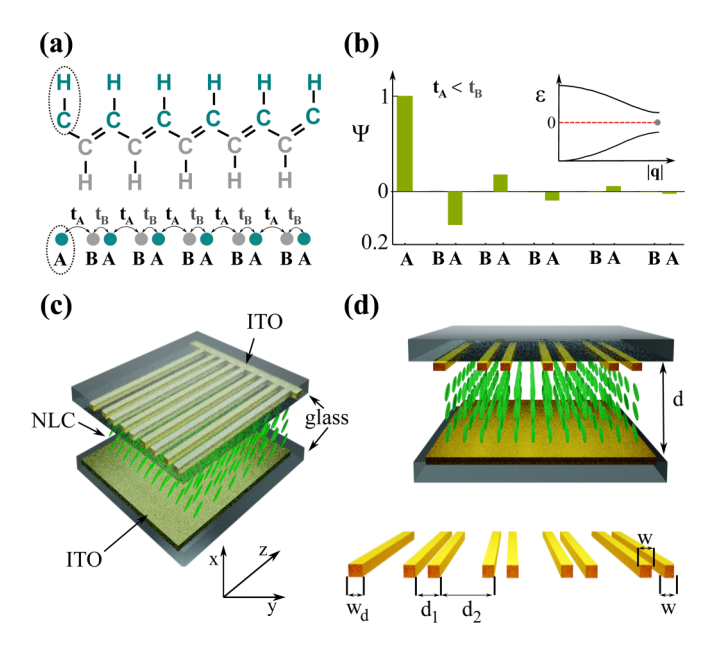


FIG. 1. The schematic of the Su-Schrieffer-Heeger model for trans-polyacetylene host and its potential implementation in a discrete liquid-crystal platform. (a) Chemical form showing the two-site unit-cell structure (A and B) with the carbon defect marked with a dashed circle. The tight-binding model representation of hopping electrons with strength t_A and t_B is shown at the bottom. (b) The bar plot on the right represents the wave function ψ for the edge state with the inset depicting the full band structure. The planar liquid-crystal cell with ITO electrodes as a platform for the SSH model where d represents the cell thickness, w and w_d are the electrode thicknesses, and d_1 , d_2 are the distances between electrodes is shown in panels (c) and (d).

 M_A and M_B represent on-site energy offsets. This model can be readily implemented in photonics using a 1D waveguide lattice with two different nearest neighbor coupling coefficients κ_1 and κ_2 . From coupled-mode theory, one finds that the corresponding evolution dynamics in this array is given by

$$i\frac{d}{dz}\psi_n + \beta_n\psi_n + \kappa_1\psi_{n-1} + \kappa_2\psi_{n+1} = 0, \tag{2}$$

where ψ_n represents the modal field amplitude and β_n is the propagation constant for waveguide site n. Here, for convenience, we assume that all sites involved are characterized by the same propagation constant. The same SSH model can be directly realized by using a nematic liquid crystal platform. For this case, we consider the NLC cell depicted in Fig. 1(c), where an AC electric field is imposed externally through the patterned electrodes in order to induce molecular orientation, which will, in turn, create a periodic waveguide system. The cell consists of a thin film of nematic liquid crystal of thickness d placed between two glass plates, which provide planar anchoring for molecules in the direction of light propagation. The electrodes in the lower and upper plates are made of indium tin oxide (ITO). In contrast to previous works where discrete light propagation in LCs was studied [27,28], here the upper electrode pattern features a double spacing with two separation distances d_1 and d_2 . Furthermore, these separations can also vary in the z direction. Consequently, the electricfield-induced waveguides will follow the same pattern. In our configuration, all but one electrodes have the same widths w, as shown in Fig. 1(c). The width of the left edge electrode chosen such that $w_d > w$, ensures that all local modes of each waveguide share approximately the same propagation constant.

The orientation of the molecules in the LC cell is determined by the externally applied AC field and by the electric field of the optical beam itself. For an extraordinary polarized optical beam, the molecular orientation angle θ can be obtained from the following equation [29]:

$$\Delta\theta + \frac{\sin(2\theta)}{2K} \left(\Delta\varepsilon_{lf} |E_x|^2 + \frac{\Delta\varepsilon}{2} |E|^2 \right) = 0, \quad (3)$$

where K is the effective elastic constant [30], while $\Delta \epsilon_{lf}$ and $\Delta \epsilon$ stand for the low- and high-frequency dielectric anisotropy, respectively. On the other hand, E represents the E component of the electric field associated with extraordinary polarized beam propagating in the LC cell while E_{E} is the low-frequency field from the biased electrodes. The E_{E} field can be determined from the corresponding potential E after solving Laplace's equation in this anisotropic medium:

$$\sum_{ii=x,v,z} \frac{\partial}{\partial ii} \left(\varepsilon_{ii} \frac{\partial}{\partial ii} V \right) = 0, \tag{4}$$

where ε_{ii} denotes diagonal components of the electric permittivity tensor [31]. In the absence of linear absorption effects, the evolution of the optical beam (propagating predominantly along the z axis), is described by the following wave equation [32–34]:

$$2ik_o n(\theta_o) \left(\frac{\partial E}{\partial z} + \tan \delta(\theta) \frac{\partial E}{\partial x}\right) + D_x \frac{\partial^2 E}{\partial x^2} + (\theta) \frac{\partial^2 E}{\partial y^2} + k_o^2 [n^2(\theta) - n^2(\theta_o)]E = 0, \tag{5}$$

where $k_o = 2\pi/\lambda_0$, $\delta(\theta)$ is the walk-off angle along the beam axis, θ_0 is the initial molecular orientation (in the absence of light), $D_x = \cos^2\theta + \gamma^2\sin^2\theta$ is the diffraction coefficient across z, and $n(\theta) = (\cos^2\theta/n_o^2 + \sin^2\theta/n_e^2)^{-1/2}$ is an effective index of refraction for the x-polarized (i.e., extraordinary) light beam. Here, n_0 and n_e represent ordinary and extraordinary refractive indexes, respectively and $\gamma^2 = n_e^2/n_o^2$. Assumption of the single elastic constant in Eq. (3) and restriction of the director movement to the single plane greatly simplifies the formal description of the response of the liquid crystal. We checked that it nevertheless gives results that agree very well with the full vectorial model involving all elastic constants (K_{11}, K_{22}, K_{33}) provided $K = \frac{K_{11} + K_{33}}{2}$ [31].

For demonstration purposes, let us now consider two examples where the SSH model is implemented in a discrete NLC platform, as depicted in Figs. 2(a) and 2(b). In both configurations, the LC cell parameters such as the separation between glass plates $d=2~\mu m$, the electrodes' width $w=2~\mu m$ and $w_d=2.35~\mu m$, and the interspace $d_1=6.8~\mu m$ and $d_2=4~\mu m$ are invariant along the propagation direction. At this point, the nonlinear effects are negligible since the arrays operate in the low power regime at a wavelength $\lambda=1.55~\mu m$. After applying external voltage, the electric field from the electrodes reorients the molecules such that the

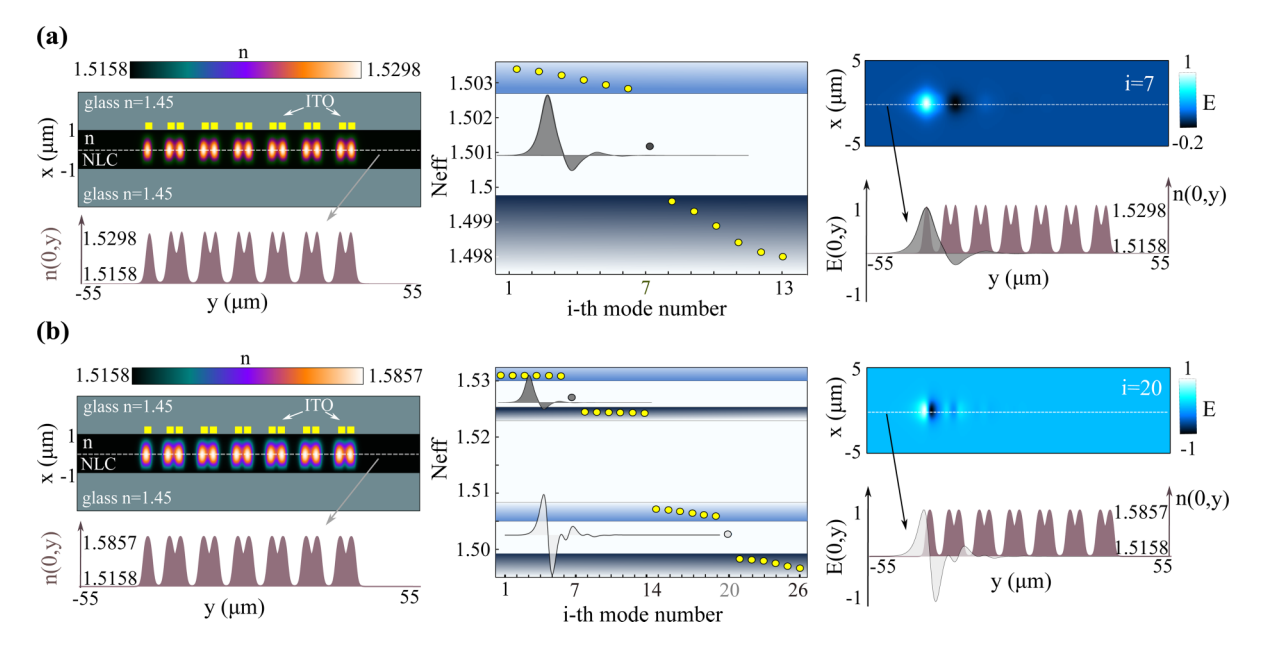


FIG. 2. The SSH model in a discrete NLC platform based on thirteen waveguides operating at $\lambda=1.55~\mu\mathrm{m}$ induced through the biasing with the voltage of (a) 0.94 V and (b) 1.15 V applied to the electrodes. The left panels show the refractive index distribution in the xy plane. In the middle panel the numerically extracted band structures for two configurations are presented. The right panels in (a) and (b) depict the optical field distribution of the topological states in the xy plane and the cross sections at x=0 of the edge modes together with the refractive index distributions. The parameters used in this design are $w=2~\mu\mathrm{m}$, $w_d=2.35~\mu\mathrm{m}$, $d=2~\mu\mathrm{m}$, $d=2.8~\mu\mathrm{m}$, d

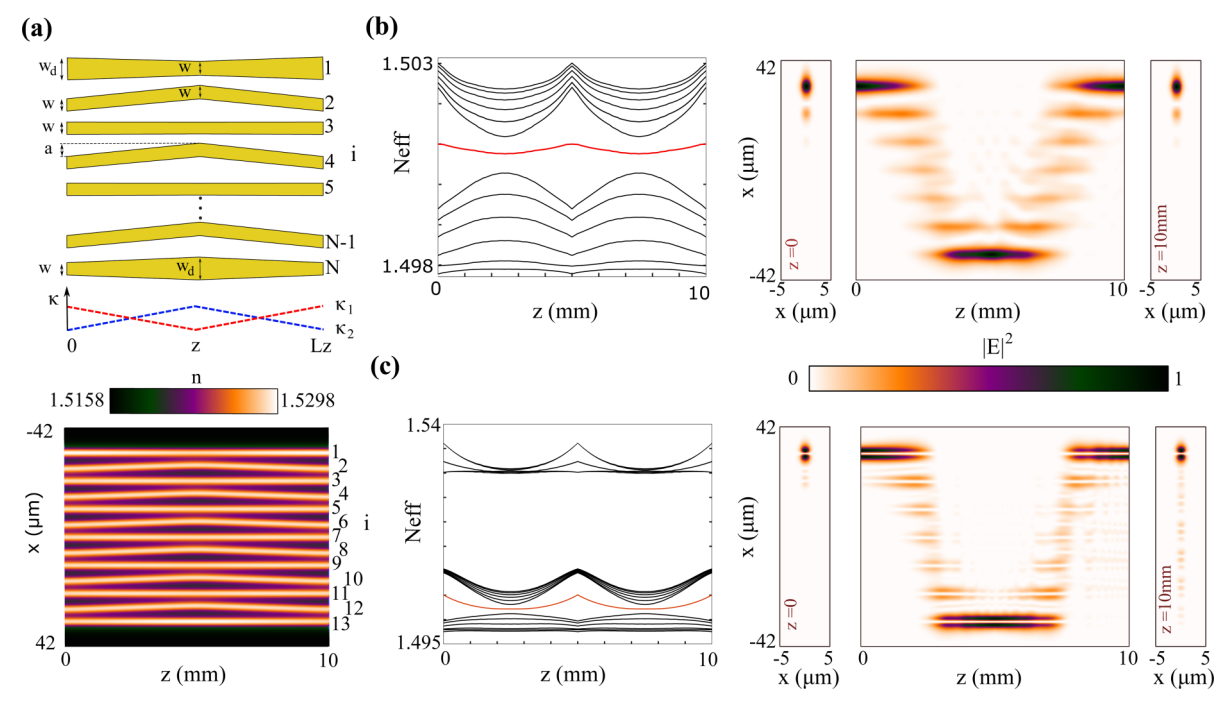


FIG. 3. The topological Thouless pumping scheme in a discrete NLS platform. (a) The schematic shape of the ITO electrodes are shown for $w=2~\mu\mathrm{m}$ and $w_d=2.35~\mu\mathrm{m}$. Every second electrode counting from the upper side changes linearly its position along the z direction between $\pm 1.4~\mu\mathrm{m}$ from the central point where the distance between electrodes is equal $(d_1=d_2=5.4~\mu\mathrm{m})$. The middle panel shows schematically the two varying couplings coefficients κ_1 and κ_2 in a coupling paths. The bottom panel depicts the slowly varying refractive index distribution in z after applying a finite voltage, forming 13 waveguide arrays. For lower biasing voltage (0.94 V) these waveguides are single-moded while they support two modes for higher bias (1.15 V). (b) The left panel depicts the numerically extracted evolution of the linear spectrum of the system as a function of distance z (a full cycle of the Thouless pump with the topologically protected state is marked in red). The right panels show that the input topological edge mode adiabatically switches between states, during linear evolution, before returning to its initial state at the output when the structure is induced at 0.94 V. (c) The analogical full cycle of the Thouless pump scheme but this time apply for a topological edge mode consisting of the second-order states (1.15 V).

extraordinary refractive index locally increases. As a result, a spatially periodic refractive index distribution is formed as shown in Figs. 2(a) and 2(b). The discrete optical lattice consists of 13 waveguides, as shown in Fig. 1(a). The separation distance between the waveguides directly translates into two different coupling strengths κ_1 and κ_2 . Here, we consider two cases. In the first scenario, after applying the external voltage (0.94 V) to the electrodes each of the waveguides is single-moded. Such structure supports 13 supermodes and a topological edge mode whose eigenvalue is located in the middle of the band gap [see Fig. 2(a)]. In the second case, after applying the external voltage (1.15 V) each of the waveguides is double-moded. The corresponding spatial refractive index distribution is shown in Fig. 2(b). In contrast to the former case, the system has two separate sub-bands and supports in total 26 supermodes and two topological edge modes. The first 13 supermodes including a topological edge mode with the highest eigenvalues are built from the first-order modes of the single waveguide. The successive 13 supermodes with another topological edge mode are constructed from the second-ordertype states. Again the eigenvalue of these topological states is still located in the middle of each sub-band gap [Fig. 2(b)].

As we indicated earlier, the topologically protected modes of the 1D SSH array exhibit no transport properties. The situation radically changes under a topological Thouless pumping protocol. In our discrete platform, the shape and orientation of the electrodes are periodically altered along the z direction, as shown in Fig. 3(a). After applying the external voltage, the LC molecular orientation establishes again a lattice of 13 waveguides [Fig. 3(b)]. However, now the refractive index distribution is varying in both the z and y direction in order to introduce the required Thouless pumping. In particular, only the position of every second waveguide slowly and periodically varies along the z direction. The separation between waveguides varies adiabatically, from d_1 to d_2 in the first half of the period and from d_2 to d_1 in the second. In addition, the width of the two outer electrodes vary with distance z to ensure that all local modes of each waveguide share approximately the same propagation constant at a given z. At low optical beam powers (linear regime) such a waveguide lattice exhibits in z periodically dependent coupling strengths $\kappa_1(z)$ and $\kappa_2(z)$ as shown schematically in the left panel of Fig. 3(a). The Hamiltonian operator describing the system is now z-dependent leading to a z evolution of its spectrum, as shown in the left panels in Figs. 3(b) and 3(c) for a complete cycle of the Thouless pump. It is worth noticing that the Hamiltonian operator at the input (z = 0) is the same as that depicted in Figs. 2(a) and 2(b). The corresponding edge modes [Figs. 3(b) and 3(c)] launched into the system now displays transport properties. The light is adiabatically switched from the edge state at i = 1at z = 0 to the edge state that occupies the waveguide number i = 13 at $z = L_z/2$ and subsequently returns to the initial site i = 1 at $z = L_z$. Notice that the transport process does not depend on whether the lattice operates at the lowest-order mode [Fig. 3(c)] or a higher-order mode [Fig. 3(d)].

Next, we utilize the topological Thouless pumping scheme under strong nonlinear conditions. To this end, we use the same parameters as in Fig. 3(c), but restrict the propagation to the distance $z = L_z/2 = 5$ mm. In such a configuration, at low powers (0.1 mW), the topologically protected edge state

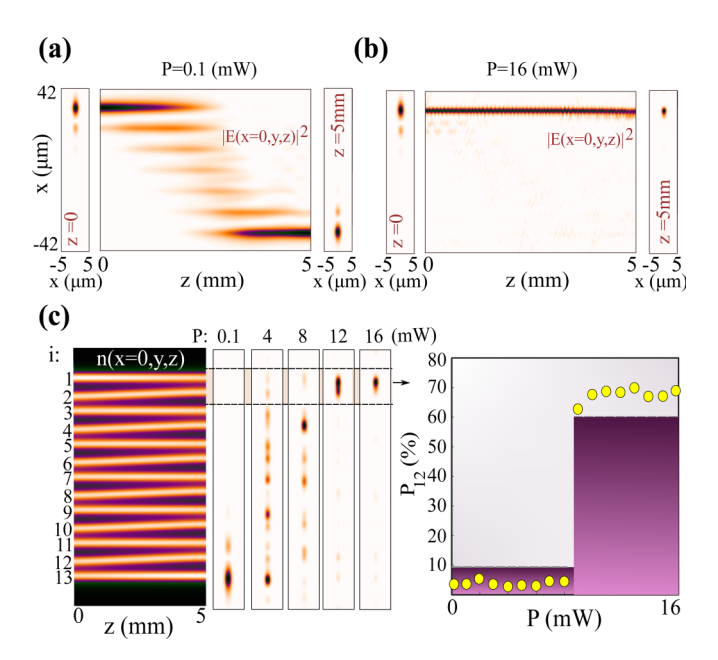


FIG. 4. The field evolution in a two-level all-optical switching arrangement that utilizes a topological Thouless pumping scheme with broken chiral symmetry. (a) Evolution of an excited topological edge mode with optical power of 0.1 mW. (b) Nonlinear propagation with the same excitation conditions and input power 16 mW. (c) A threshold all-optical switching based on the ratio between the output power confined in the first two waveguides (P_{12}) to the total input power (P).

launched at i = 1 displays transport properties, as depicted in Fig. 4(a). Again at the output, a nontrivial edge state forms, with the energy irreversibly remaining in the waveguide i =13. On the other hand, at higher power level (16 mW) and with the same input conditions, the light breaks the chiral symmetry and propagates in a self-induced nonlinear waveguide (as a discrete soliton). As a result, at the output, we observe most of the energy confined in the first channel (i = 1). In this respect, all-optical switching occurs between the nontrivial edge state and its trivial nonlinear defect counterpart. In such configuration, the two level all-optical switching can be observed at approximately P = 9 mW of the initial power P as shown in Fig. 4(c). For $P \ge 9$ mW, the system switches to its upper state with more than 60% of the power confined in the first two waveguides, while below threshold P < 9 mW, the system occupies the lowest state.

In conclusion, we investigated a nematic liquid crystal SSH topological model operating under the action of a Thouless pumping scheme. In doing so, we judiciously designed electrode structures to observe a topological edge mode consisting of the superposition of the first- and second-order states of the single waveguide. By utilizing a Thouless protocol we observed edge to edge light transport at low power levels. On the other hand, at higher powers, the transport is frustrated by light-induced nonlinear defect states, thus giving rise to robust all-optical switching.

This work was partially supported by The Qatar National Research Fund (Grant NPRP13S-0121-200126), the Polish National Science Center (Contract No.

UMO-2013/08/A/ST3/00708), and the Polish Ministry of Science and Higher Education (1654/MOB/V/2017/0), the Polish National Science Center (2016/22/M/ST2/00261), the Bodossaki Foundation, DARPA (D18AP00058), the Office of Naval Research (N00014-20-1-2522, N00014-20-1-2789, N00014-16-1-2640, N00014-18-1-2347, and N00014-19-1-2052), FOTECH-1 project ("Electrically driven waveguiding systems in LC:PDMS structures")

granted by the Warsaw University of Technology under the program Excellence Initiative: Research University (ID-UB), the Army Research Office (W911NF-17-1-0481), the Air Force Office of Scientific Research (FA9550-14-1-0037 and FA9550-20-1-0322), the National Science Foundation (CBET 1805200, ECCS 2000538, ECCS 2011171, DMR-1420620), the US-Israel Binational Science Foundation (BSF; 2016381), and the Simons Foundation (Simons Grant 733682).

- [1] F. D. M. Haldane, Model for a Quantum Hall Effect without Landau Levels: Condensed-Matter Realization of the "Parity Anomaly," Phys. Rev. Lett. **61**, 2015 (1988).
- [2] C. L. Kane and E. J. Mele, Quantum Spin Hall Effect in Graphene, Phys. Rev. Lett. **95**, 226801 (2005).
- [3] M. König, S. Wiedmann, C. Brüne, A. Roth, H. Buhmann, L. W. Molenkamp, X.-L. Qi, and S.-C. Zhang, Quantum spin Hall insulator state in HgTe quantum wells, Science 318, 766 (2007).
- [4] S.-Y. Xu, I. Belopolski, D. S. Sanchez, C. Zhang, G. Chang *et al.*, Experimental discovery of a topological Weyl semimetal state in tap, Sci. Adv. 1, e1501092 (2015).
- [5] B. Q. Lv, H. M. Weng, B. B. Fu, X. P. Wang, H. Miao, J. Ma, P. Richard, X. C. Huang, L. X. Zhao, G. F. Chen, Z. Fang, X. Dai, T. Qian, and H. Ding, Experimental Discovery of Weyl Semimetal TaAs, Phys. Rev. X 5, 031013 (2015).
- [6] G. Jotzu, M. Messer, R. Desbuquois, M. Lebrat, T. Uehlinger, D. Greif, and T. Esslinger, Experimental realization of the topological Haldane model with ultracold fermions, Nature (London) 515, 237 (2014).
- [7] Z. Wang, Y. Chong, J. D. Joannopoulos, and M. Soljačić, Observation of unidirectional backscattering-immune topological electromagnetic states, Nature (London) 461, 772 (2009).
- [8] Y. G. Liu, P. S. Jung, M. Parto, D. N. Christodoulides, and M. Khajavikhan, Gain-induced topological response via tailored long-range interactions, Nat. Phys. 17, 704 (2021).
- [9] A. B. Khanikaev, S. H. Mousavi, W.-K. Tse, M. Kargarian, A. H. MacDonald, and G. Shvets, Photonic topological insulators, Nat. Mater. 12, 233 (2013).
- [10] M. Hafezi, S. Mittal, J. Fan, A. Migdall, and J. Taylor, Imaging topological edge states in silicon photonics, Nat. Photonics 7, 1001 (2013).
- [11] M. C. Rechtsman, J. M. Zeuner, Y. Plotnik, Y. Lumer, D. Podolsky, F. Dreisow, S. Nolte, M. Segev, and A. Szameit, Photonic Floquet topological insulators, Nature (London) 496, 196 (2013).
- [12] M. A. Bandres, S. Wittek, G. Harari, M. Parto, J. Ren, M. Segev, D. N. Christodoulides, and M. Khajavikhan, Topological insulator laser: Experiments, Science 359, eaar4003 (2018).
- [13] W. P. Su, J. R. Schrieffer, and A. J. Heeger, Solitons in Polyacetylene, Phys. Rev. Lett. 42, 1698 (1979).
- [14] D. J. Thouless, Quantization of particle transport, Phys. Rev. B 27, 6083 (1983).
- [15] Y. E. Kraus, Y. Lahini, Z. Ringel, M. Verbin, and O. Zilberberg, Topological States and Adiabatic Pumping in Quasicrystals, Phys. Rev. Lett. 109, 106402 (2012).

- [16] M. Verbin, O. Zilberberg, Y. Lahini, Y. E. Kraus, and Y. Silberberg, Topological pumping over a photonic Fibonacci quasicrystal, Phys. Rev. B **91**, 064201 (2015).
- [17] A. Cerjan, M. Wang, S. Huang, K. P. Chen, and M. C. Rechtsman, Thouless pumping in disordered photonic systems, Light: Sci. Appl. 9, 178 (2020).
- [18] Q. Fu, P. Wang, Y. V. Kartashov, V. V. Konotop, and F. Ye, Non-linear Thouless pumping: solitons and transport breakdown, arXiv:2110.14472.
- [19] M. Jürgensen, S. Mukherjee, and M. C. Rechtsman, Quantized nonlinear Thouless pumping, Nature (London) **596**, 63 (2021).
- [20] V. Brosco, L. Pilozzi, R. Fazio, and C. Conti, Non-Abelian Thouless pumping in a photonic lattice, Phys. Rev. A 103, 063518 (2021).
- [21] H. Abbaszadeh, M. Fruchart, W. van Saarloos, and V. Vitelli, Liquid-crystal-based topological photonics, Proc. Natl. Acad. Sci. USA 118, e2020525118 (2021).
- [22] M. Peccianti, A. De Rossi, G. Assanto, A. De Luca, C. Umeton, and I. Khoo, Electrically assisted self-confinement and waveguiding in planar nematic liquid crystal cells, Appl. Phys. Lett. 77, 7 (2000).
- [23] Y. V. Izdebskaya, V. G. Shvedov, P. S. Jung, and W. Krolikowski, Stable vortex soliton in nonlocal media with orientational nonlinearity, Opt. Lett. 43, 66 (2018).
- [24] D. Smirnova, D. Leykam, Y. Chong, and Y. Kivshar, Non-linear topological photonics, Appl. Phys. Rev. **7**, 021306 (2020).
- [25] S. Xia, D. Song, N. Wang, X. Liu, J. Ma, L. Tang, H. Buljan, and Z. Chen, Topological phenomena demonstrated in photorefractive photonic lattices, Opt. Mater. Express 11, 1292 (2021).
- [26] M. Parto, S. Wittek, H. Hodaei, G. Harari, M. A. Bandres, J. Ren, M. C. Rechtsman, M. Segev, D. N. Christodoulides, and M. Khajavikhan, Edge-Mode Lasing in 1D Topological Active Arrays, Phys. Rev. Lett. 120, 113901 (2018).
- [27] A. Fratalocchi, G. Assanto, K. A. Brzdakiewicz, and M. A. Karpierz, Discrete propagation and spatial solitons in nematic liquid crystals, Opt. Lett. 29, 1530 (2004).
- [28] A. Fratalocchi, G. Assanto, K. A. Brzdakiewicz, and M. A. Karpierz, Discrete light propagation and self-trapping in liquid crystals, Opt. Express 13, 1808 (2005).
- [29] G. Assanto and M. Peccianti, Spatial solitons in nematic liquid crystals, IEEE J. Quantum Electron. 39, 13 (2003).

- [30] I. C. Khoo, H. Li, and Y. Liang, Optically induced extraordinarily large negative orientational nonlinearity in dye-doped liquid crystal, IEEE J. Quantum Electron. 29, 1444 (1993).
- [31] F. A. Sala and M. A. Karpierz, Modeling of molecular reorientation and beam propagation in chiral and non-chiral nematic liquid crystals, Opt. Express **20**, 13923 (2012).
- [32] J. Fleck and M. Feit, Beam propagation in uniaxial anisotropic media, J. Opt. Soc. Am. **73**, 920 (1983).
- [33] A. Alberucci, A. Piccardi, M. Peccianti, M. Kaczmarek, and G. Assanto, Propagation of spatial optical solitons in a dielectric with adjustable nonlinearity, Phys. Rev. A **82**, 023806 (2010).
- [34] P. S. Jung, Y. V. Izdebskaya, V. G. Shvedov, D. N. Christodoulides, and W. Krolikowski, Formation and stability of vortex solitons in nematic liquid crystals, Opt. Lett. **46**, 62 (2021).